analytical chemistry

Article

Cite This: Anal. Chem. 2018, 90, 4354−4362

pubs.acs.org/ac

Potential of Near-Infrared Chemical Imaging as Process Analytical Technology Tool for Continuous Freeze-Drying

Davinia Brouckaert,[†] Laurens De Meyer,[†] Brecht Vanbillemont,[†] Pieter-Jan Van Bockstal,[†] Joris Lammens,[‡] Séverine Mortier,[†,§] Jos Corver,[∥] Chris Vervaet,[‡] Ingmar Nopens,[§] and Thomas De Beer*[,†]

[†]Laboratory of Pharmaceutical Process Analytical Technology, Ghent University, Ottergemsesteenweg 460, 9000 Ghent, Belgium

[‡]Laboratory of Pharmaceutical Technology, Ghent University, Ottergemsesteenweg 460, 9000 Ghent, Belgium

[§]BIOMATH, Ghent University, Coupure Links 653, 9000 Ghent, Belgium

[∥]RheaVita, High Tech Campus 9, NL 5656 AE Eindhoven, The Netherlands

ABSTRACT: Near-infrared chemical imaging (NIR-CI) is an emerging tool for process monitoring because it combines the chemical selectivity of vibrational spectroscopy with spatial information. Whereas traditional near-infrared spectroscopy is an attractive technique for water content determination and solid-state investigation of lyophilized products, chemical imaging opens up possibilities for assessing the homogeneity of these critical quality attributes (CQAs) throughout the entire product. In this contribution, we aim to evaluate NIR-CI as a process analytical technology (PAT) tool for at-line inspection of continuously freeze-dried pharmaceutical unit doses based on spin freezing. The chemical images of freeze-dried mannitol samples were resolved via multivariate curve resolution, allowing us to visualize the distribution of mannitol solid forms throughout the entire cake. Second, a mannitol-sucrose formulation was lyophilized with variable drying times for inducing changes in water content. Analyzing the corresponding chemical images via principal component analysis, vial-to-vial variations as well as within-vial inhomogeneity in water content could be detected. Furthermore, a partial least-squares regression model was constructed for quantifying the water content in each pixel of the chemical images. It was hence concluded that NIR-CI is inherently a most promising PAT tool for continuously monitoring freeze-dried samples. Although some practicalities are still to be solved, this analytical technique could be applied in-line for CQA evaluation and for detecting the drying end point.

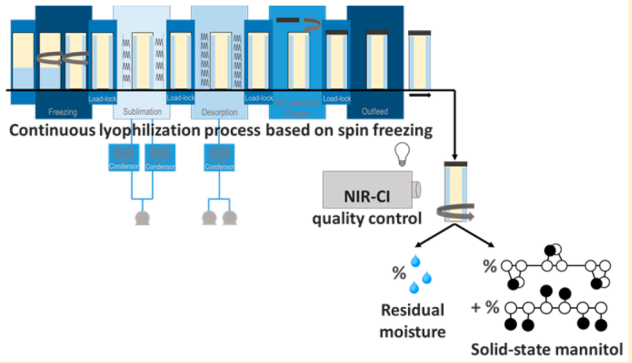

Freeze-drying or lyophilization is a popularly applied drying process for increasing product stability. The gentle low-temperature drying method enables enhancing the preservation of a wide range of materials, ranging from food items and microorganisms to biological products and pharmaceuticals.[1−4]

Focusing on the pharmaceutical sector, the traditional batch-wise lyophilization practice has some important drawbacks from an industrial point of view. Freeze-drying is a time-consuming and costly technique with a high footprint, often exhibiting uncontrolled vial-to-vial and batch-to-batch end product variability.[3,5−11] From a regulatory point of view, such uncontrolled variability is not desired. With the launch of the PAT initiative in 2004, the United States Food and Drug Administration (FDA) has opened the way to innovative pharmaceutical development, manufacturing, and quality control based on the quality by design (QbD) concept.[12] By demanding enhanced process knowledge and extensive process control, pharmaceutical companies and regulatory bodies worldwide have realized that the current batch-wise manufacturing practice often lacks cost-effectiveness, in-depth knowledge, and profound quality control.[13] Therefore, the integration of continuous manufacturing lines is promoted in view of assuring consistent quality, shortening processing times, and decreasing the ecological footprint.[14]

To come to grips with this, an innovative continuous freeze-drying concept was proposed.[7,8] This concept starts with a continuous spin freezing step, where the vials, which are filled with a liquid formulation, are rotated rapidly along their longitudinal axis. Meanwhile, a flow of cold sterile gas around the spinning vial induces the ice nucleation and subsequent freezing. This way, the resulting frozen product is distributed in a thin layer over the longitudinal vial wall surface, in contrast with traditional freeze-drying, where the lyophilized cake is packed at the bottom of the container. By increasing the surface area of the product and decreasing the layer thickness, the total process time is reduced. Scale-up is realized by simply

Received: September 6, 2017
Accepted: March 12, 2018
Published: March 12, 2018

DOI: 10.1021/acs.analchem.7b03647
Anal. Chem. 2018, 90, 4354−4362

duplicating the already validated system, making complete reoptimization and revalidation of the process unnecessary.[7,8]

Furthermore, the continuous freeze-drying procedure offers the opportunity to monitor and control quality attributes of the freeze-dried product at the individual vial level. Employing process analytical technology (PAT) tools, the lyophilized product can rapidly and nondestructively be analyzed both after and during the freeze-drying cycle. This is in contrast with conventional quality control, where only a handful of vials per batch are sampled and submitted to slow off-line laboratory analyses. Such quality-by-testing strategies on randomly collected samples are in conflict with the latest QbD and PAT guidelines from the regulatory authorities, which request a guaranteed quality in each released vial, as individually sampled vials may not be representative for the entire batch.[13,15] Moreover, these off-line techniques are labor-intensive and time-consuming and cannot offer real-time information on the lyophilized product. In addition, they are often destructive or use toxic reagents, such as the Karl Fischer titration for residual moisture determination. Therefore, Raman and near-infrared (NIR) spectroscopy have been investigated as noninvasive PAT tools for improving process efficiency and guaranteeing final product quality.[11,16−21] Both techniques have proven to offer fast and real-time information on critical quality attributes such as water to ice conversion, product crystallization, solid-state characterization, residual moisture determination, protein unfolding, and protein−lyoprotectant interaction behavior. However, the introduction of such spectroscopic equipment in a conventional batch freeze-drying unit is inconvenient from an engineering point of view. On the industrial scale, it is practically speaking unachievable to monitor and control every single individual vial because the traditional freeze-drying equipment consists of large shelves containing hundreds of closely packed products. Moreover, the main limitation inherent to these process analyzers is that only a fraction of the vial can be monitored and intravial variability is thus not taken into account.[16,17]

Therefore, this study focuses on the use of near-infrared chemical imaging (NIR-CI), which combines the chemical information from the spectral features in the NIR region with the spatial information on the constituent distribution derived from the pixel-to-pixel spectral variation.[22] This way, an image is collected from the entire lyophilized cake and a NIR spectrum is acquired for each pixel in that image. This allows us to inspect not only vial-to-vial variability but also within-vial variability. Using the continuous freeze-drying concept, each individual vial can be examined entirely by the hyperspectral camera. As the penetration depth of the NIR spectrometer closely approaches the product layer thickness, it is fair to say that this setup allows a 100% inspection of the lyophilized formulations. This would again be unattainable in a traditional batch lyophilization process. Hence, it is the combined benefit of continuous freeze-drying via the spin freezing concept and entire cake visualization through hyperspectral imaging that makes the proposed PAT strategy revolutionary and innovative. Moving away from the traditional batch manufacture practice and introducing a PAT methodology that combines vibrational spectroscopy with spatial information confers a promising production approach for assuring fast and reliable lyophilization with consistent vial-to-vial and within-vial quality control.

The general objective was to demonstrate the applicability of NIR-CI for investigating the homogeneity of some critical quality attributes (CQAs) of freeze-dried products throughout the lyophilized cake after spin freezing and subsequent drying. Therefore, the entire sample surface of rotating lyophilized model formulations was inspected. First, it was aimed at evaluating the solid-state properties of mannitol in freeze-dried formulations, as the physical state of crystalline components can affect the reconstitution time as well as the chemical and physical stability of the final product.[17,23] Hence, it was intended to identify the different solid forms of mannitol and to visualize their distribution throughout the entire lyophilized cake using multivariate curve resolution (MCR). Second, the residual water content in a series of mannitol-sucrose freeze-dried samples was assessed. This is another essential CQA because remaining water affects the shelf life, the physical and chemical stability, and the overall quality of pharmaceutical products.[24,25] Finally, it is practically unachievable in batch freeze-drying to precisely detect when all ice and when all water is removed from each vial. Because in continuous freeze-drying based on spin freezing the product is spread in a thin layer around the vial wall and the sublimation front is moving in the direction of that wall, analyzing the entire formulation with an NIR camera during drying could allow a contactless and accurate detection of the drying end point without affecting the drying process itself. All currently used sensors and drying monitoring technologies in batch freeze-drying do not allow accurate drying end point detection in each vial or influence the drying process of the monitored vials, making the monitored unit doses unrepresentative for the nonmonitored ones. To first evaluate this opportunity at-line, a number of samples was freeze-dried with varying drying times, hence inducing fluctuations in water content. It was then investigated whether these variations could be captured by NIR-CI and whether the distribution of the water within one sample could contribute to an improved knowledge on the spin freezing process.

MATERIALS AND METHODS

Materials and Formulations. Two simple model formulations were lyophilized using the continuous freeze-drying concept in view of investigating their solid-state properties and residual water content (Table 1). The first formulation, employed for solid-state examination, was a 2.9 mL of 5% (w/v) D-mannitol (ABC Chemicals, Belgium) solution. D-Mannitol, further referred to as simply "mannitol", is a popularly employed excipient in freeze-dried formulations.[16,26] In its amorphous form, mannitol can serve as a lyoprotecant through the formation of a hydration shell around protection-requiring molecules such as proteins. Moreover, mannitol is often formulated as a bulking agent because the presence of its crystalline forms results in elegant cakes by providing structural support.[26,27] The purchased powder consisted of mannitol's crystalline β-polymorph and was used as received. To collect a

Table 1. Studied Sample Formulations and the Variations in Primary Drying Time Applied during Freeze-Drying

batch	mannitol (mg/mL)	sucrose (mg/mL)	primary drying time (h)
M1	50	0	12
M2	50	0	6
MS1	25	25	12
MS2	25	25	3
MS3	25	25	2
MS4	25	25	1.5
MS5	25	25	1

DOI: 10.1021/acs.analchem.7b03647
Anal. Chem. 2018, 90, 4354−4362

reference spectrum of δ-mannitol, this polymorph was obtained from Merck (Germany). Two mannitol batches, respectively, referred to as M1 and M2 were freeze-dried. They both consisted of 5% β-mannitol in water and differed solely in primary drying time utilized during lyophilization (Table 1). Second, 2.9 mL of mannitol-sucrose (5% w/v total dry product) samples were lyophilized with varying primary drying times to create fluctuating residual water levels. The weight ratio between mannitol and sucrose was 1:1, so each solution contained 25 mg/mL sucrose (Sigma-Aldrich, Germany) and 25 mg/mL β-mannitol (ABC Chemicals, Belgium). Table 1 includes the changes in continuous freeze-drying process parameters applied to induce variations in dryness of the final product. Five batches were produced, each consisting of four samples. All liquid formulations were prepared in 10R type I glass vials (Schott, Germany).

Spin Freezing and Drying. The continuous freeze-drying concept, described extensively by De Meyer et al.,[7] starts with a continuous freezing step, in which the glass vial was rotated rapidly (~2900 rpm) along its longitudinal axis. Hence, the present liquid formulation was spread across the vial wall, followed by immersion into liquid nitrogen to solidify the solution. In contrast with traditional freeze-drying, where the lyophilized cake is packed at the bottom of the vial, the resulting frozen product was distributed in a thin layer over the longitudinal vial surface (Figure 1). In combination with the enlarged surface area, this thin product layer allows us to significantly increase the sublimation rate. The frozen product was then immediately transferred to an aluminum vial holder, which was precooled to −40 °C.[7] Subsequently, the holder was placed inside the drying chamber of a conventional Lyobeta 25 freeze-dryer (Telstar, Spain), whose shelves were also precooled to −40 °C. Afterward, vacuum was introduced (150 μbar) and the shelf temperature set point was changed to 20 °C. The energy for sublimation provided by the shelf was conducted to the spin frozen vials through the aluminum holders.[7] To obtain a completely dry product, a primary drying time of 12 hours was used. For the vials with a higher water content, the drying process was interrupted earlier (Table 1) when the pressure value indicated by the Pirani sensor dropped and started approaching the one from the Baratron capacitance (MKS Instruments, USA) pressure sensor. It should be noted that such long drying times are somewhat in conflict with the reduced processing times envisaged by continuous manufacturing but are due to the temporary employment of a conventional freeze-dryer for drying of the spin frozen vials. At the end of the freeze-drying process, the chamber was vented with dry nitrogen gas and the vials were stoppered and capped.

Figure 1. Schematic representation of the spin freezing step in a continuous freeze-drying process.[7] Reproduced with permission from ref 7. Copyright Elsevier 2015.

Raman Spectroscopy. In view of obtaining reference data for the NIR-CI analyses, the solid-state properties of the mannitol samples were investigated via Raman spectroscopy. Raman spectra were collected with a Rxn1 spectrometer (Kaiser Optical Systems, USA), equipped with a fiber-optic noncontact probe with a spot size of 150 μm and an air-cooled CCD detector. The laser wavelength was the 785 nm line from an Invictus NIR diode laser. A laser power of 400 mW was used. Five distinct regions of each mannitol batch (M1 and M2) were sampled and three Raman spectra were acquired of each segment of the cake. All spectra were recorded with an exposure time of five seconds and averaged over ten scans by the HoloGRAMS software (Kaiser Optical Systems, USA). Analysis of the acquired Raman spectra was performed using PLS_Toolbox version 8.2.1 (Eigenvector Research, USA) running on MATLAB R2016a (The MathWorks, USA). Standard normal variate (SNV) scaling was applied to the 1000−1170 cm^{-1} spectral range. This allows for comparison of the sample spectra to the reference spectra of all four solid-state conditions of mannitol, as described by De Beer et al.[16] Several solid-state conditions of mannitol in freeze-dried formulations have been described: the anhydrous α-, β-, and δ-polymorphs and the hemihydrate form. The predominant outcome after lyophilization is influenced by several parameters, such as the sample formulation and process conditions.[16,17,26] Inspecting the Raman spectra of M1 and M2, it was determined which of them was present in the lyophilized mannitol cakes.

Karl Fischer Titration. As a reference method for water content determination in the mannitol-sucrose samples, Karl Fischer titrations were performed. A V30 volumetric Karl Fischer titrator (Mettler Toledo, Switzerland) with Hydranal-Composite 5 reagent (Sigma-Aldrich, Germany) was used. Prior to sample analysis, the concentration of the Karl Fischer titrant was determined as well as the water content of the Hydranal dry methanol (Sigma-Aldrich, Germany). Then, a known volume of dry methanol was added to each sample vial and left to equilibrate. From the dissolved cake, a known mass was removed using a syringe and injected into the titration cell. The water content of the pure methanol was subtracted from the result. The samples were analyzed in duplicate (two different vials from the same batch) and the mean value of the replicates was employed as the reference value for the water content.

NIR Chemical Imaging. The freeze-dried vials were inspected with a push-broom hyperspectral imaging system (VLNIR, Specim, Finland). This line-scanning chemical imager is made up of an Imspector 17E spectrograph and scans a row of 320 spatial pixels at a time. The incoming light from each pixel in the spectral range of 900−1700 nm is dispersed onto one column of the 320 × 256-pixel InGaAs detector (12-bit read-out, thermo-electrically cooled). To obtain a chemical image of the entire cake surface after spin freeze-drying, the spectrograph was placed horizontally on a bench, facing a rotating vial. The complete cake was hence inspected through the side of the vial, by rotating the sample perpendicular to the beam of the NIR spectrometer, using a customized spinning device (Figure 2). The vial turned with a speed of 1 rpm and spectral data were acquired with an exposure time of 10 ms and a scanning speed of 15 Hz. A halogen bulb (400 W) illuminated the sample.

Multivariate Data Analysis. *Image Preprocessing.* After each sample collection, a white standard I_0 and a dark current d were measured. These spectral acquisitions were performed by

DOI: 10.1021/acs.analchem.7b03647
Anal. Chem. 2018, 90, 4354−4362

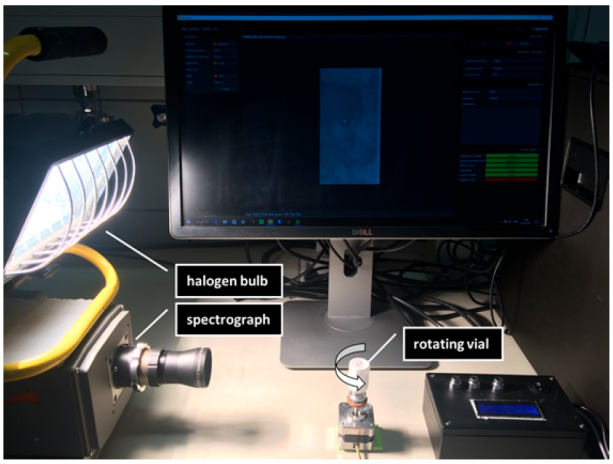

Figure 2. Experimental setup of the NIR-CI instrument during freeze-dried sample inspection. The lyophilized cake was examined through the side of the vial, while the sample was rotating perpendicularly to the spectrograph.

placing a white Teflon tile at the vial position and closing the shutter of the spectrograph, respectively. The sample measurement intensity I could hence be converted from counts to spectroscopic pseudoabsorbance units A via eq 1

$$A = -\log[(I - d)/(I_0 - d)] \quad (1)$$

This radiometric one-point calibration automatically corrects for lamp drift, inhomogeneous illumination, and optical or detector proficiency because the absorbance is calculated pixel-wise.[28] Spectral (pre)processing of the obtained chemical imaging data was further performed using MATLAB (The MathWorks, USA) routines provided by Amigo et al.[29,30]

Solid-State Analysis. For assessing the solid-state properties of mannitol, the NIR-CI data of the M1 and M2 vials were preprocessed by cropping the spectral range from 1376 until 1640 nm, applying Savitzky−Golay smoothing (second-order polynomial, window width = 23) and performing SNV correction. This way, undesirable light scattering effects and instrumental noise in the spectral data are minimized.[29,31]

Augmented MCR was then carried out to estimate the relative abundance of mannitol's solid forms throughout the lyophilized cakes. This resolution algorithm allows decomposing the original raw data matrix D of the freeze-dried vials into a bilinear model

$$D = CS^T + E \quad (2)$$

where C embodies the stretched concentration profiles and S^T represents the matrix of pure solid form spectra. The error matrix E contains the unmodeled residuals.[22,32,33]

Using MCR-ALS, the decomposition of the data matrix D into the bilinear model is executed by means of a constrained alternating least-squares (ALS) optimization of the C and S^T matrices. The application of this algorithm involves three main steps. First, the number of constituents should be determined. In this study, the number of compounds in the raw data set was considered to be equal to the number of mannitol solid forms detected via Raman spectroscopy. Second, initial estimates are to be generated. Accordingly, the pure component spectra of the identified solid forms were employed for this purpose. Finally, C and S^T are iteratively optimized until convergence is achieved. This completion is reached when no significant variation is obtained among the results of consecutive cycles.[22,32,33]

No a priori knowledge is required to resolve data sets into their bilinear models. However, by introducing the available information through the employment of constraints, the ambiguity in the resolved profiles is greatly reduced and the chemical meaning of the recovered distribution maps is ensured. In this study, non-negativity in the concentration profile C was imposed, as well as closure (i.e., mass balance in concentrations). Another approach to minimize the ambiguity and to improve the definition of the distribution maps and pure spectra of the components is the introduction of local rank information. Therefore, the augmentation of the original sample with more images was proposed by Juan et al. to enhance the selectivity.[32,33] This approach has been applied successfully in content uniformity studies[34−36] and was performed here by expanding the data matrix D of the lyophilized vials with NIR-CI data of mannitol's pure solid forms. Consequently, the correspondence among the species constraint was applied during ALS optimization to provide information on the presence or absence of the different species in the augmented data matrix.

The MCR analysis was performed using the MCR-ALS GUI created by Jaumot et al.,[37,38] running on MATLAB R2016b (The MathWorks, USA). The percentage of lack of fit (%LOF) between the obtained results and the original data was calculated via

$$\%\mathrm{LOF} = 100 \times \sqrt{\frac{\sum_{x=1}^{X}\sum_{y=1}^{Y}\sum_{\lambda=1}^{\lambda} e_{xy\lambda}^2}{\sum\sum\sum d_{xy\lambda}^2}} \quad (3)$$

where $e_{xy\lambda}^2$ and $d_{xy\lambda}^2$ represent the $xy\lambda$-th terms of the residuals and original data set, respectively.[34]

Water Content Analysis. Given the high number of applications described in literature, it is generally acknowledged that NIR spectroscopy is a suitable technique for fast water content determination in freeze-dried samples. This is due to the strong water absorption bands in the NIR region of the electromagnetic spectrum. For quantification purposes, most authors employ the combination band observed around 1920 nm to achieve accurate, precise, robust, and sensitive predictive models. Because the NIR-CI instrumentation employed during this research is limited to the spectral range from 900 to 1700 nm, the OH stretching overtone near 1400−1450 nm was investigated in view of obtaining insight into the residual water content of the lyophilized mannitol-sucrose vials.[20,27,39−42]

The spectral data of each chemical image were cropped in the range of 1350−1470 nm, and SNV correction was applied to them to compensate for baseline offset. This was then followed by second-derivative preprocessing (second-order polynomial, window width = 19), a commonly applied transformation technique for emphasizing the spectral features of water-related data.[24,29,39,41,42]

Primarily, exploratory image analysis was performed through principal component analysis (PCA). Visualizing the distribution maps of the first principal component, it was verified whether the increase in residual water content from MS1 to MS5 could be detected using the given spectral range and preprocessing. Furthermore, it was evaluated whether the distribution of the water within each lyophilized cake was homogeneous.

DOI: 10.1021/acs.analchem.7b03647
Anal. Chem. 2018, 90, 4354−4362

Because PCA simply displays the systematic variation in the data and cannot offer any quantitative information, a partial least-squares (PLS) regression model was constructed. This was performed by regressing the median spectrum of each vial acquisition against its corresponding water level, as obtained by Karl Fischer titration. Although the number of samples was limited, this quantification model may provide an estimation of the amount of water present in each pixel of the analyzed vials.

RESULTS AND DISCUSSION

Raman Spectroscopy. Raman spectra were collected from the lyophilized mannitol cakes of M1 and M2 for comparison to the reference spectra of all four solid-state conditions described in literature, acquired from De Beer et al.[16] (Figure 3A). Figure 3B exhibits that the Raman spectra of both freeze-dried mannitol samples (M1 and M2) show great resemblance with the reference spectrum of β-mannitol, while some spectral features of δ-mannitol can be observed as well. This is highlighted by acquiring Raman spectra of β- and δ-mannitol raw materials, as displayed in Figure 3B. It was hence concluded that both lyophilized mannitol samples contain a mixture of β- and δ-mannitol solid forms, while no signs of α-mannitol or hemihydrate spectral features can be detected.

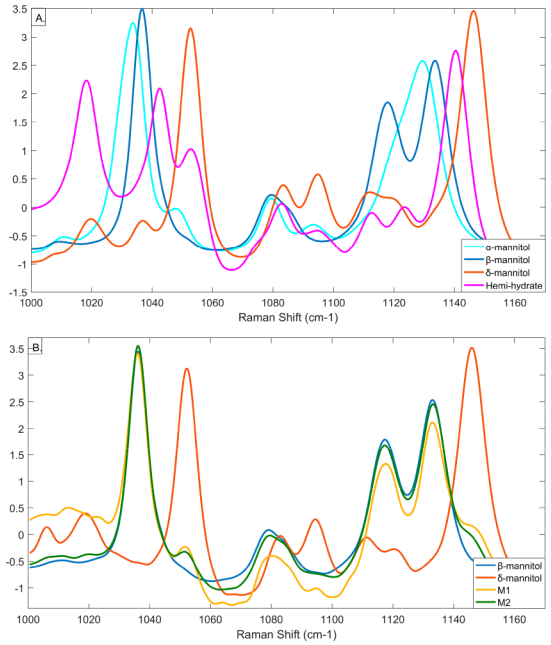

Figure 3. (A) Reference Raman spectra of the four mannitol forms (α, β, δ, and hemihydrate), as described by De Beer et al.[16] (B) Raman spectra of the lyophilized mannitol samples M1 (yellow) and M2 (green) after SNV preprocessing. Spectral features of the mannitol β- (blue) and δ- (red) polymorph can be identified.

Karl Fischer Titration. Table 2 lists the residual water content of the freeze-dried mannitol-sucrose samples, as obtained by Karl Fischer titration. The displayed values are the average of two independent concentration determinations per batch. Applying a primary drying time of 12 h, the MS1 batch yields a water content of ~0.5%. By gradually decreasing the drying time of the mannitol-sucrose samples, a progressive increase in water level from 2.0 to 8.7% is observed for the other batches (MS2 until MS5).

Table 2. Water Content of the Lyophilized Mannitol-Sucrose Samples As Determined by the Karl Fischer Reference Method[a]

sample	residual water (%(m/m))
MS1	0.54
MS2	2.04
MS3	3.74
MS4	4.11
MS5	8.73

[a]Displayed value (%(m/m)) is the average of two vial titrations per batch.

NIR Chemical Imaging. The unprocessed image of a scanned vial is presented in Figure 4. On the y axis, the chemical image is built up of 910 lines, which together cover the entire circumference of the vial. Each line consists of 320 pixels along the longitudinal axis of the spinning vial (x axis). The left side of the image represents the upper part of the sample, while the right side corresponds to the bottom of the container. For each of the 291 200 pixels, a NIR spectrum is present in the z axis. Pixels with high relative intensities are displayed in red, while lower intensities are colored blue.

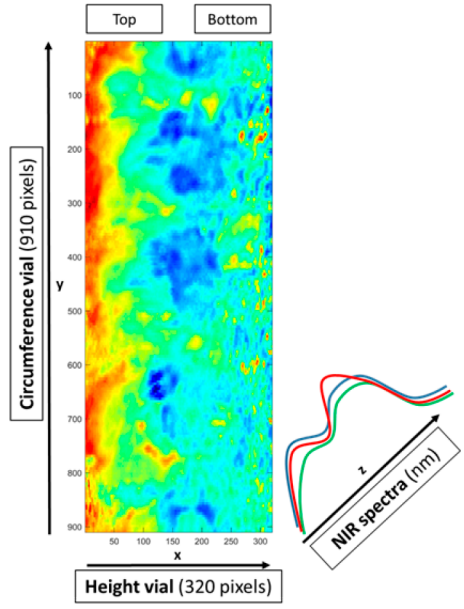

Figure 4. Unprocessed image of a lyophilized sample as obtained by the NIR chemical imager. The x and y axes, respectively, represent the height and full circumference of the freeze-dried cake. A near-infrared spectrum is obtained for each pixel in the image, as represented in the z axis. The color scale shows the highest pixels in red, while the lowest pixels are blue.

Multivariate Data Analysis. *Solid-State Analysis.* Because the reference Raman spectra show no signs of mannitol's α-polymorph or hemihydrate form, only the β- and δ-solid-state were considered during MCR analysis. NIR-CI data were collected from their raw mannitol powder material, as received by the supplier. Subsequently, the chemical image of both pure polymorphs was preprocessed in accordance with the lyophilized vial data, applying Savitzky–Golay smoothing and SNV scaling to the spectral range from 1376 until 1640 nm. The median spectrum of their respective preprocessed chemical image was then employed as an initial estimate of the pure

DOI: 10.1021/acs.analchem.7b03647
Anal. Chem. 2018, 90, 4354–4362

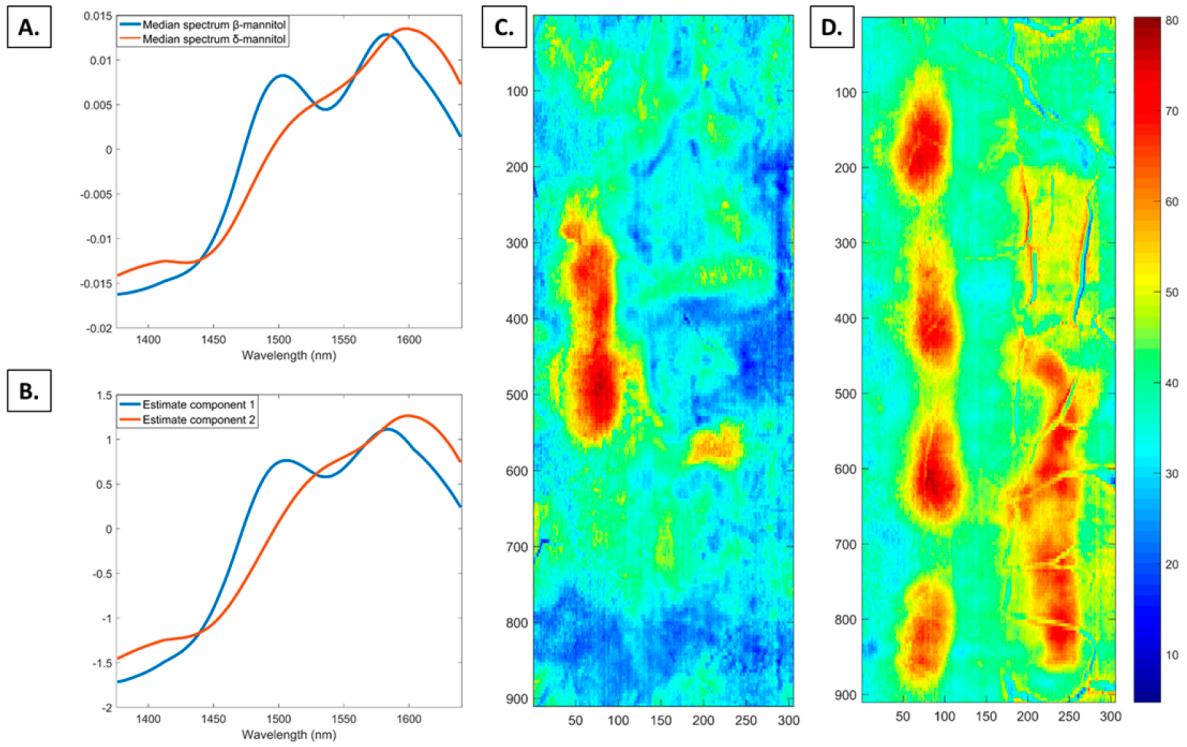

Figure 5. (A) Initial estimates provided to the MCR-ALS GUI: median spectrum of pure β- (blue) and δ- (red) mannitol reference measurement. (B) Estimates of the two MCR model components at the ALS optimum. Component 1 (blue) corresponds to the β-mannitol reference, while component 2 (red) shows spectral similarity with the δ-polymorph. (C) Reconstructed image of mannitol sample M1 showing the concentration distributions of β- (blue) and δ- (red) mannitol. (D) Reconstructed image of mannitol sample M2 showing the concentration distribution of β- (blue) and δ- (red) mannitol.

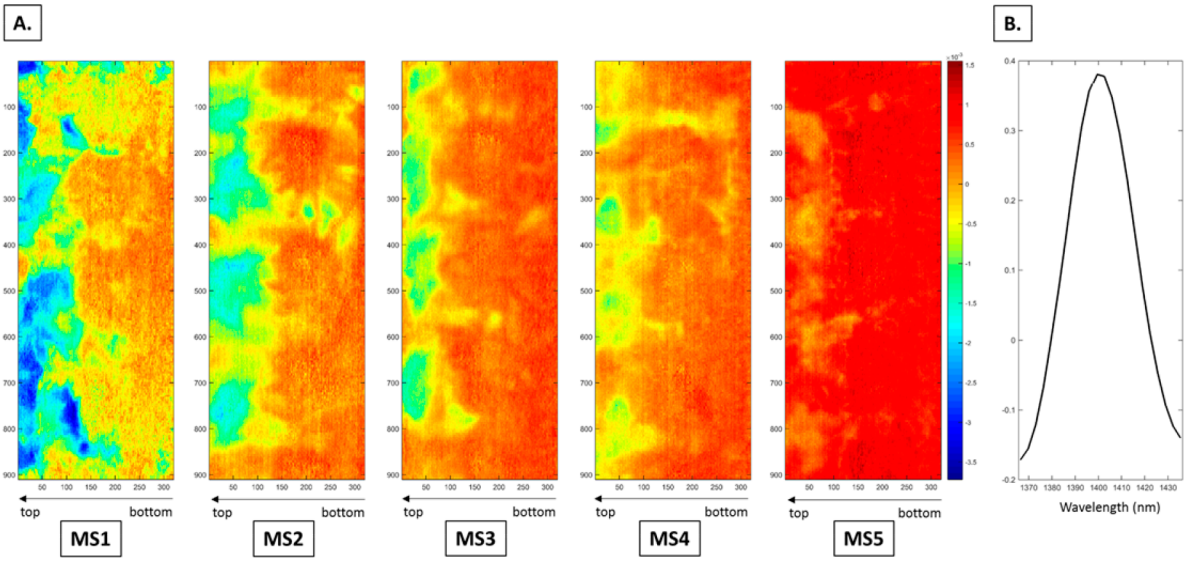

Figure 6. (A) Reconstructed PCA scores images of mannitol-sucrose samples MS1 to MS5 illustrating variations from low (blue) to high (red) scores values, equivalent to, respectively, low and high water levels. (B) Corresponding loading plot of the first principal component.

component contributions to the resolution model (Figure 5A). Hereafter, a multiset structure was created, by column-wise augmentation of the preprocessed and unfolded images acquired for both pure polymorphs, followed by the ones of the M1 and M2 freeze-dried sample. Loading this data matrix into the MCR-ALS GUI, together with the initial estimates and predefined constraints, ALS optimizations were then initiated. Convergence was achieved at the second iteration, resulting in an MCR model that explains 99.95% of the total variance and has a lack of fit of 2.212%. This denotes that there is no ambiguity in the resolution results of this two-component MCR model. The estimated constituents at the ALS optimum are displayed in Figure 5B. It can clearly be witnessed that the estimate of component 1 corresponds well with the reference spectrum of β-mannitol, while the reference spectrum of δ-mannitol resembles the estimate of component 2. This high similarity between the spectral profiles obtained via augmented MCR and the pure spectra confirms the correct development

DOI: 10.1021/acs.analchem.7b03647
Anal. Chem. 2018, 90, 4354−4362

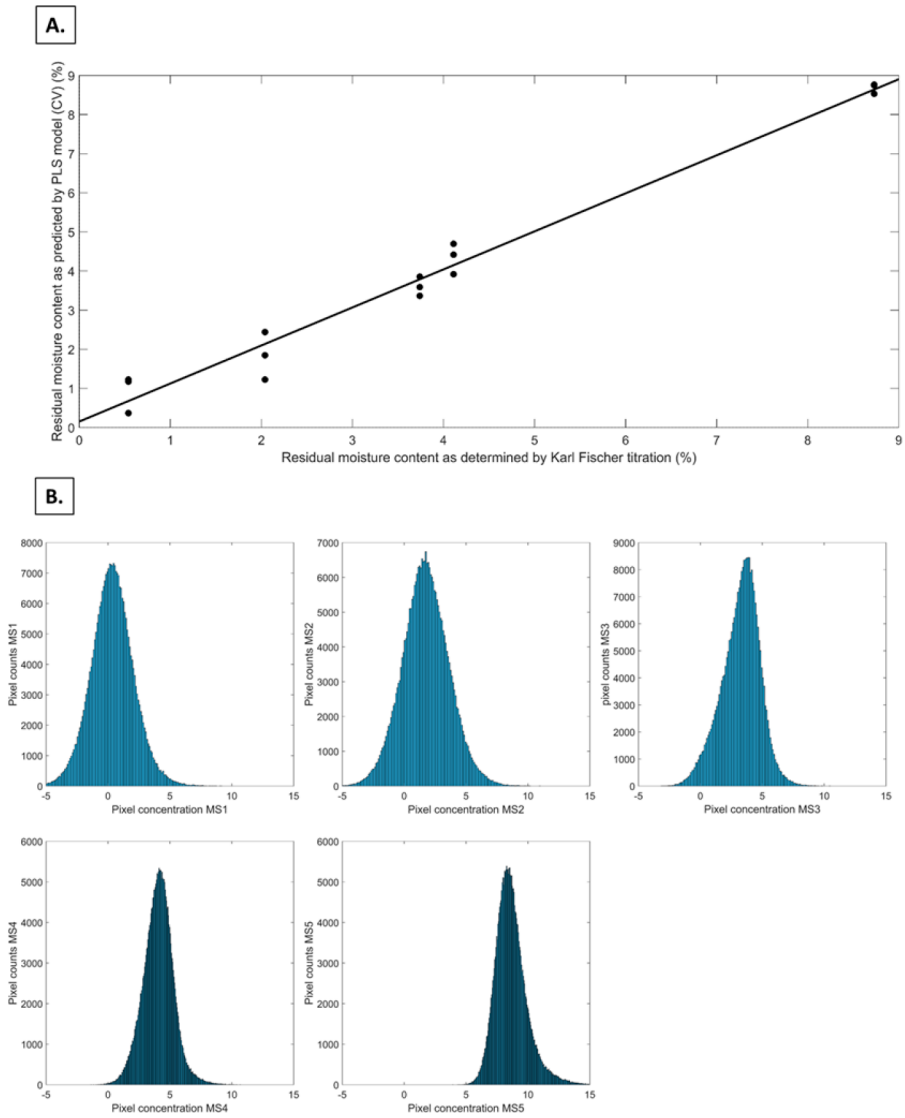

Figure 7. (A) Observed versus predicted plot of the PLS calibration model, constructed by regressing the median spectra of the chemical images against the Karl Fischer results. (B) Histograms of the water concentrations obtained for the five samples (MS1 to MS5) by means of PLS regression.

and good performance of the model. The reconstituted images of mannitol samples M1 and M2 are displayed in Figure 5C,D, respectively. The employed color scale links high intensities of red to high relative abundance of component 2 (δ-mannitol), while blue pixels mark the relative abundance of component 1 (β-mannitol). As a result, distinct regions of δ-mannitol can be noticed, embedded in an overall mainly β-mannitol cake. It is generally acknowledged that several factors, such as concentration, cooling rate, formulation, and process parameters, influence the solid-state outcome of mannitol after lyophilization.[23,43] Under the current process conditions, a combination of both β- and δ-mannitol is thus obtained. This alteration occurs during the freezing step, in which mannitol has a strong tendency to crystallize. The detected within-vial differences in solid form are most likely caused by an unequal freezing rate, which can be ascribed to the impediment of an aluminum vial holder employed during spin freezing. Although the freezing conditions of M1 and M2 are identical, the conversion to δ-mannitol seems to be more pronounced in M2. This is most likely due to a difference in temperature of this vial holder, as for spin-freezing the first vial of a batch, the holder is still at room temperature, while by the fourth vial, the temperature has already significantly decreased before connecting the vial to its holder.

Water Content Analysis. Exploring the chemical images of the lyophilized mannitol-sucrose samples (MS1 to MS5) through PCA, it is denoted that the first principal component (PC1, explaining 80.94% of the variance) represents the water content in the lyophilized cakes (Figure 6). The increasing water level from MS1 to MS5 is clearly depicted from the increasing intensity of the color scale, ranging from blue for the driest regions to dark red for the vial with the shortest drying time. Furthermore, a difference in color scale is denoted within each vial, indicating that, whatever the primary drying conditions, the bottom of the cake contains more residual water in comparison with the top. An explanation for this trend can be found in the fact that during spin freezing a rotating device with a maximal velocity of 2900 rpm was employed. This results in an inhomogeneous frozen product, where the cake at the bottom of the vial is slightly thicker than the cake near the

DOI: 10.1021/acs.analchem.7b03647
Anal. Chem. 2018, 90, 4354−4362

top of the container. This dissimilarity in layer thickness between top and bottom (Δl) can be calculated via

$$\Delta l = \frac{h \cdot g}{w^2 \cdot \sqrt{r_{v,i}^2 - \frac{V}{\pi \cdot h}}} \quad (4)$$

where h represents the height of the spin frozen cake (m), g is the gravitational acceleration (9.81 m/s^2), w denotes the angular velocity (rad/s), $r_{v,i}$ is the inner radius of the vial (m), and V corresponds to the filling volume (m^3). Using the in this study applied experimental process parameters, a Δl of 0.34 mm is obtained. This small difference in layer thickness results in slightly lower sublimation rates at the bottom compared with the top of the vial, which is correlated with a higher water content near the bottom of the vial. Minimization of this effect could be obtained by increasing the rotational speed during spin freezing. Raising the rotational speed from 2900 to 5000 rpm, for instance, yields a Δl of only 0.11 mm. However, in the current setup, rotational speeds higher than 2900 rpm were not achievable.

The PLS calibration model, constructed by regressing the median spectra of the mannitol-sucrose images against their reference water content values, is visualized in Figure 7A. Three sample acquisitions per lyophilized vial were employed for regression against the off-line Karl Fischer data. Random cross-validation with 7 splits and 15 iterations yields a root-mean-square error of cross-validation (RMSECV) of 0.4093, and a good fit between the measured and predicted values is observed. It should, however, be noted that the predictions of an external, fully independent data set should be evaluated to properly validate the calibration model.

The regression model displayed in Figure 7A was then employed to predict the water content in each pixel of the lyophilized mannitol-sucrose samples. Histograms were created by plotting the pixel counts of the obtained concentrations for each sample (Figure 7B). It is observed that the distributions present a Gaussian shape and that the central value of each histogram is well in accordance with the Karl Fischer results. On the contrary, the distribution of the histograms is quite wide. Because the homogeneity of the examined compound is represented by the width of the obtained distribution, this is expected, due to the unequal layer thickness. Looking at the profile for MS4, for example, the pixel concentrations range from fully dry (0% residual water near the top of the cake) to ~10% water at the bottom of the vial. The predictions of the mannitol-sucrose cakes with the longest drying times show negative concentration values at their driest pixels. This is physically impossible and can be ascribed to an insufficient coverage of the concentration range by the calibration model. Extra mannitol-sucrose samples should be lyophilized with deviating dryness degrees to further optimize the regression model and validate it using a fully independent sample set.

Broader Applicability. NIR-CI could be a valuable tool for addressing CQAs of continuously freeze-dried pharmaceutical unit doses based on spin freezing. It was demonstrated that chemical imaging allows determination of water content and solid-state characterization in the entire lyophilized cake with a high spatial resolution. Furthermore, this PAT could potentially be applied for detecting in a contactless way (and without affecting the process itself) the end of drying as the sublimation front of the spin frozen samples is moving in the direction of the camera. However, some practicalities are still to be overcome before introducing this technology in a continuous freeze-drier.

First, in view of acquiring high-quality hyperspectral images of the entire lyophilized vials, it is crucial to obtain optimum angles of detection between the sample and the spectrograph. The position of the rotating vial should thus be consistent and perfectly perpendicular to the detector to collect robust and reliable spectroscopic data.

Moreover, quartz or tungsten halogen sources are the standard NIR light sources for illuminating solid samples. However, because these halogen bulbs tend to heat up the samples, their use in a continuous freeze-drying unit may disturb the process. The employment of other compact, low-voltage light sources should hence be considered, taking into account that lamp power, stability, and lifetime are critical specifications. Options to evaluate could be LEDs (light-emitting diodes) or laser-driven light sources as well as diffuse illumination.

Third, in view of taking the proposed strategy in-line for real-time control of critical process parameters such as sublimation rate, some additional mechanical challenges are to be faced, concerning the dimensions of the hyperspectral imaging system, the speed of data acquisition, and the robustness of the spectroscopic equipment to endure the lyophilization process conditions. Because the chemical analyzer cannot be implemented in a GMP (good manufacturing practices) freeze-drying chamber, a setup should be created that allows the collection of NIR chemical images through an appropriate window. Furthermore, the spectral acquisition parameters should be adapted in view of corresponding the speed of data collection to the rotational speed employed for drying in the vacuum oven. Currently, the construction of one vial image takes 1 min, but this can be optimized in view of reaching a higher speed by fine-tuning the scanning speed and exposure time.

■ CONCLUSIONS

NIR-CI was evaluated as a PAT tool for assessing the homogeneity of two CQAs in lyophilized cakes after spin freezing. Using Raman spectroscopy as a reference method, two mannitol solid forms were detected and their distribution throughout the freeze-dried samples was visualized via MCR of the chemical images. Furthermore, a mannitol-sucrose model formulation was freeze-dried in five-fold, applying different primary drying times for inducing batch-to-batch variations in residual water content. PCA of their chemical images showed that NIR-CI is able to detect these varying degrees of dryness and to reveal within-vial inhomogeneity in water content. Regressing the spectroscopic data against the reference water concentration from Karl Fischer titration, an estimation of the water quantity in each pixel of the NIR-CI image was obtained. It is hence concluded that although some practicalities are still to be overcome in view of a broader applicability, the combination of spectroscopic and spatial information conferred by NIR-CI can be valuable in assessing the final product quality of continuously freeze-dried pharmaceutical unit doses after spin freezing.

■ AUTHOR INFORMATION

Corresponding Author

*Tel: +32 9 264 80 97. E-mail: thomas.debeer@ugent.be.

DOI: 10.1021/acs.analchem.7b03647
Anal. Chem. 2018, 90, 4354−4362

ORCID

Davinia Brouckaert: 0000-0002-8296-2013
Pieter-Jan Van Bockstal: 0000-0002-0363-3618

Notes

The authors declare no competing financial interest.

REFERENCES

(1) Williams, N. A.; Polli, G. P. *J. Pharm. Sci. Technol.* **1984**, *38*, 48−60.
(2) Tsinontides, S. C.; Rajniak, P.; Pham, D.; Hunke, W. A.; Placek, J.; Reynolds, S. D. *Int. J. Pharm.* **2004**, *280*, 1−16.
(3) Kasper, J. C.; Winter, G.; Friess, W. *Eur. J. Pharm. Biopharm.* **2013**, *85*, 162−169.
(4) Geidobler, R.; Winter, G. *Eur. J. Pharm. Biopharm.* **2013**, *85*, 214−222.
(5) Kasper, J. C.; Friess, W. *Eur. J. Pharm. Biopharm.* **2011**, *78*, 248−263.
(6) Tang, X. C.; Pikal, M. J. *Pharm. Res.* **2004**, *21*, 191−200.
(7) De Meyer, L.; Van Bockstal, P. J.; Corver, J.; Vervaet, C.; Remon, J. P.; De Beer, T. *Int. J. Pharm.* **2015**, *496*, 75−85.
(8) Van Bockstal, P.-J.; De Meyer, L.; Corver, J.; Vervaet, C.; De Beer, T. *J. Pharm. Sci.* **2017**, *106*, 71−82.
(9) Liu, J.; Viverette, T.; Virgin, M.; Anderson, M.; Dalal, P. *Pharm. Dev. Technol.* **2005**, *10*, 261−272.
(10) Barresi, A. A.; Pisano, R.; Rasetto, V.; Fissore, D.; Marchisio, D. L. *Drying Technol.* **2010**, *28*, 577−590.
(11) Kauppinen, A.; Toiviainen, M.; Korhonen, O.; Aaltonen, J.; Järvinen, K.; Paaso, J.; Juuti, M.; Ketolainen, J. *Anal. Chem.* **2013**, *85*, 2377−2384.
(12) United States Food and Drug Administration. Guidance for Industry. *PAT — A Framework for Innovative Pharmaceutical Development, Manufacturing and Quality Assurance*. http://www.fda.gov/downloads/drugs/guidances/ucm070305.pdf (accessed Aug 8, 2017).
(13) Hinz, D. C. *Anal. Bioanal. Chem.* **2006**, *384*, 1036−1042.
(14) United States Food and Drug Administration. *FDA Perspective on Continuous Manufacturing*. www.fda.gov (accessed Aug 8, 2017).
(15) European Medicines Agency. *ICH Guideline Q8 (R2) on Pharmaceutical Development*; London, 2017.
(16) De Beer, T. R. M.; Vercruysse, P.; Burggraeve, A.; Quinten, T.; Ouyang, J.; Zhang, X.; Vervaet, C.; Remon, J. P.; Baeyens, W. R. G. *J. Pharm. Sci.* **2009**, *98*, 3430−3446.
(17) Romero-Torres, S.; Wikström, H. *PDA J. Pharm. Sci. Technol.* **2007**, *61*, 131−145.
(18) De Beer, T. R. M.; Alleso, M.; Goethals, F.; Coppens, A.; Vander Heyden, Y.; Lopez De Diego, H.; Rantanen, J.; Verpoort, F.; Vervaet, C.; Remon, J. P.; Baeyens, W. R. G. *Anal. Chem.* **2007**, *79*, 7992−8003.
(19) Rosas, J. G.; de Waard, H.; De Beer, T.; Vervaet, C.; Remon, J. P.; Hinrichs, W. L. J.; Frijlink, H. W.; Blanco, M. *J. Pharm. Biomed. Anal.* **2014**, *97*, 39−46.
(20) Trnka, H.; Palou, A.; Panouillot, P. E.; Kauppinen, A. R. I.; Toiviainen, M.; Grohganz, H.; Alcalà, M.; Juuti, M.; Ketolainen, J.; Rantanen, J. *J. Pharm. Sci.* **2014**, *103*, 2839−2846.
(21) Pieters, S.; De Beer, T.; Kasper, J. C.; Boulpaep, D.; Waszkiewicz, O.; Goodarzi, M.; Tistaert, C.; Friess, W.; Remon, J. P.; Vervaet, C.; Vander Heyden, Y. *Anal. Chem.* **2012**, *84*, 947−955.
(22) Salzer, R.; Siesler, H. W. *Infrared and Raman Spectroscopic Imaging*, 2nd ed.; Wiley-VCH: Weinheim, Germany, 2014.
(23) Kim, A. I.; Akers, M. J.; Nail, S. L. *J. Pharm. Sci.* **1998**, *87*, 931−935.
(24) Lin, T. P.; Hsu, C. C. *PDA J. Pharm. Sci. Technol.* **2002**, *56*, 196−205.
(25) Muzzio, C. R.; Dini, N. G.; Simionato, L. D. *Braz. J. Pharm. Sci.* **2011**, *47*, 289−297.
(26) Mehta, M.; Bhardwaj, S. P.; Suryanarayanan, R. *Eur. J. Pharm. Biopharm.* **2013**, *85*, 207−213.
(27) Cao, W.; Mao, C.; Chen, W.; Lin, H.; Krishnan, S.; Cauchon, N. *J. Pharm. Sci.* **2006**, *95*, 2077−2086.
(28) Boldrini, B.; Kessler, W.; Rebner, K.; Kessler, R. W. *J. Near Infrared Spectrosc.* **2012**, *20*, 438.
(29) Vidal, M.; Amigo, J. M. *Chemom. Intell. Lab. Syst.* **2012**, *117*, 138−148.
(30) Amigo, J. M. *Anal. Bioanal. Chem.* **2010**, *398*, 93−109.
(31) Sacré, P.; De Bleye, C.; Chavez, P.-F.; Netchacovitch, L.; Hubert, P.; Ziemons, E. *J. Pharm. Biomed. Anal.* **2014**, *101*, 123−140.
(32) de Juan, A.; Tauler, R.; Dyson, R.; Marcolli, C.; Rault, M.; Maeder, M. *TrAC, Trends Anal. Chem.* **2004**, *23*, 70−79.
(33) de Juan, A.; Tauler, R. *Crit. Rev. Anal. Chem.* **2006**, *36*, 163−176.
(34) Amigo, J. M.; Ravn, C. *Eur. J. Pharm. Sci.* **2009**, *37*, 76−82.
(35) Franch-lage, F.; Amigo, J. M.; Skibsted, E.; Maspoch, S.; Coello, J. *Int. J. Pharm.* **2011**, *411*, 27−35.
(36) Cruz, J.; Blanco, M. *J. Pharm. Biomed. Anal.* **2011**, *56*, 408−412.
(37) Jaumot, J.; Gargallo, R.; De Juan, A.; Tauler, R. *Chemom. Intell. Lab. Syst.* **2005**, *76*, 101−110.
(38) Jaumot, J.; de Juan, A.; Tauler, R. *Chemom. Intell. Lab. Syst.* **2015**, *140*, 1−12.
(39) Derksen, M. W. J.; Van De Oetelaar, P. J. M.; Maris, F. A. *J. Pharm. Biomed. Anal.* **1998**, *17*, 473−480.
(40) Stokvold, A.; Dyrstad, K.; Libnau, F. O. *J. Pharm. Biomed. Anal.* **2002**, *28*, 867−873.
(41) Zhou, G. X.; Ge, Z.; Dorwart, J.; Izzo, B.; Kukura, J.; Bicker, G.; Wyvratt, J. *J. Pharm. Sci.* **2003**, *92*, 1058−1065.
(42) Grohganz, H.; Fonteyne, M.; Skibsted, E.; Falck, T.; Palmqvist, B.; Rantanen, J. *J. Pharm. Biomed. Anal.* **2009**, *49*, 901−907.
(43) Grohganz, H.; Gildemyn, D.; Skibsted, E.; Flink, J. M.; Rantanen, J. *J. Pharm. Sci.* **2011**, *100*, 2871−2875.

DOI: 10.1021/acs.analchem.7b03647
Anal. Chem. 2018, 90, 4354−4362